Journal of Magnetic Resonance 193 (2008) 77–88

Contents lists available at ScienceDirect

Journal of Magnetic Resonance

journal homepage: www.elsevier.com/locate/jmr

An analysis of phase-modulated heteronuclear dipolar decoupling sequences in solid-state nuclear magnetic resonance

Rajendra Singh Thakur [a], Narayanan D. Kurur [b,*], P.K. Madhu [a,*]

[a] Department of Chemical Sciences, Tata Institute of Fundamental Research, Homi Bhabha Road, Colaba, Mumbai 400005, India
[b] Department of Chemistry, Indian Institute of Technology Delhi, Hauz Khas, New Delhi 110016, India

ARTICLE INFO

Article history:
Received 11 January 2008
Revised 10 April 2008
Available online 23 April 2008

Keywords:
Solid-State NMR
Heteronuclear dipolar decoupling
TPPM
SPINAL
Swept-frequency TPPM
Liquid crystal

ABSTRACT

The design of variants of the swept-frequency two-pulse phase modulation sequence for heteronuclear dipolar decoupling in solid-state NMR is reported, their performance evaluated, and compared with other established sequences like TPPM and SPINAL. Simulations performed to probe the role of the homonuclear ^{1}H–^{1}H bath show that the robustness of the decoupling schemes improves with the size of the bath. In addition, these simulations reveal that the homonuclear ^{1}H–^{1}H bath also leads to broad baselines at high MAS rates. Results from a study of the SPINAL decoupling scheme indicate that optimisation of the starting phase and phase increment improves its performance and efficiency at high MAS rates. Additionally, experiments performed on a liquid crystal display the role of the initial phase in SPINAL-64 and sequences in the SW$_f$-TPPM family.

1. Introduction

Heteronuclear dipolar decoupling combined with magic-angle spinning (MAS) is necessary to obtain narrow lines in solid-state NMR spectra of rare spins when they are coupled to abundant spins [1–3]. This is the case whilst recording ^{13}C spectra of organic compounds, amino acids, proteins, and drugs as ^{13}C is a rare spin and is dipolar coupled to the abundant ^{1}H spins. Decoupling improves resolution and is also naturally accompanied by an increase in sensitivity.

A continuous burst of radio-frequency (RF) irradiation on the ^{1}H spins, like in solution-state NMR for heteronuclear *J* decoupling, was observed to effect a certain degree of heteronuclear dipolar decoupling in solid-state NMR. This scheme, called CW decoupling [4], was used routinely till the mid 1990s when a paradigm shift occurred with the introduction of two-pulse phase modulation (TPPM) [5] after which many decoupling sequences were introduced [6–9]. A rigorous understanding of the spin interactions, higher-order terms, and cross terms with and among the various spin interactions has proved to be useful in formulating better decoupling sequences [10]. Several drawbacks of the CW scheme were also noticed with the advent of more sophisticated experimental approaches, for instance, high-speed MAS probes. It was, for example, observed that the spectral lines actually broaden out with increasing MAS frequencies contrary to expectation [10]. This is now attributed to the reduction of the homonuclear ^{1}H–^{1}H dipolar couplings with increasing MAS frequencies. Detailed description of the progress made in this problem can be found in the recent reviews [6,7].

As already mentioned TPPM [5] was the first sequence to offer considerable improvement over CW in decoupling. This scheme consists of two pulses of equal lengths (denoted by τ) which differ in phase (denoted by 2ϕ). Achieving optimum performance with TPPM involves optimisation of τ as well as ϕ. The mechanism of phase modulation in TPPM together with a criterion for efficient decoupling was worked out recently by Leskes et al. on the basis of bimodal Floquet theory [11]. It was shown that careful optimisation of τ and ϕ is needed to satisfy the decoupling conditions.

A few of the decoupling sequences introduced after TPPM that deserve merit are the following. An improvement of TPPM was introduced by Fung et al. which consists of TPPM blocks with discretely incremented phases and termed small phase incremental alteration (SPINAL) [12]. Although originally designed for static samples like liquid crystals SPINAL performs admirably for spinning samples. Based on the arguments of Leskes et al., the efficiency of this sequence can be understood in terms of its ability to satisfy decoupling conditions owing to alteration of the phases. Another modification of TPPM with continuous phase variation was proposed by Paëpe et al. named cosine modulation (CM) [13,14]. Unlike TPPM, where the phase is square-wave modulated, CM involves generating a cosine profile with different initial values and time period for optimum performance by automated iteration.

* Corresponding authors. Fax: +91 22 2280 4610 (P.K. Madhu).
E-mail addresses: nkurur@chemistry.iitd.ac.in (N.D. Kurur), madhu@tifr.res.in (P.K. Madhu).

1090-7807/$ - see front matter © 2008 Published by Elsevier Inc.
doi:10.1016/j.jmr.2008.04.024

This study was fruitful in unraveling the mechanism of decoupling, but its experimental implementation is involved. Gerbaud et al. have convoluted a Gaussian with cosine modulation to effect heteronuclear dipolar decoupling and also addressed some issues related to the robustness of decoupling sequences [15]. Khitrin et al. have designed decoupling sequences by convoluting many cosine modulations that lead to certain degree of robust performance [16]. Their semi-quantitative arguments suggested the requirement of an additional modulation on TPPM for improved heteronuclear dipolar decoupling.

An altogether different strategy for designing heteronuclear dipolar decoupling sequences was adopted by Levitt and coworkers who demonstrated a set of *C*-sequences for heteronuclear dipolar decoupling [17] based on the symmetry properties of tensorial interactions [18]. Riedel et al. have demonstrated improvement in *C*-sequences by using adiabatic pulses [8].

A conceptually distinct approach, called XiX, was adopted by Meier and coworkers [19]. Its origin could be traced to an earlier attempt by Tekely [20]. Unlike the phase-modulated sequences, the decoupling efficiency of XiX improves as the MAS frequency increases.

Recently, we have designed robust decoupling sequences for both MAS experiments [9] and static cases [21]. Our approach consisted of modulating TPPM blocks by discretely changing the duration of each block in an adiabatic fashion. The resulting scheme, swept-frequency TPPM (SW_f-TPPM), due to the adiabatic sweep was shown to generate robustness with respect to various experimental parameters. This was also exemplified in the theoretical approach based on bimodal Floquet treatment [11]. The SW_f-TPPM sequence also offers significant intensity enhancement of MQMAS spectra of quadrupolar samples and is again insensitive to misset of various experimental parameters [22].

We here report on the experimental investigation of the performance of modulated TPPM sequences under MAS and especially the role played by the depth of the phase modulation ϕ for SW_f-TPPM scheme. Simulations and experiments show that TPPM fails at high MAS rates a result which was already demonstrated for TPPM [19]. The same is true for SW_f-TPPM scheme unless the cycle time is changed or additional modulations are imposed. Experimental corroboration of the earlier observations of the optimum initial value of $\phi = 15^\circ$ in the SPINAL scheme instead of the generally accepted $\phi = 10^\circ$ in the case of static liquid crystals will also be shown. The manuscript deals with: the design strategy of various decoupling schemes on the lines of SW_f-TPPM, a revisit of the efficiency of the SW_f-TPPM decoupling scheme, probing the role of the homonuclear ^1H–^1H coupling on heteronuclear dipolar decoupling via numerical simulations, a discussion on the study of various newly designed SW_f-TPPM analogues and SPINAL, and a study of decoupling in a liquid-crystal to discern the effect of the starting phase of the sequence on the decoupling efficiency.

2. Design of the pulse sequences

A detailed study of heteronuclear dipolar decoupling was recently done by Leskes et al. laying down conditions for decoupling and looking into resonance conditions for decoupling with respect to various experimental parameters [11]. SW_f-TPPM was designed by modulating the pulse length in TPPM with tangential profile. The tangential profile ensures that the resonance conditions for decoupling are met for a range of values of the pulse duration. Other variants reported here are designed by modulating the pulse length albeit the profiles are different. These sequences are designed as variants of SW_f-TPPM by sweeping across the aforementioned resonance condition in many possible ways. Thus, we have a diversity of distribution of frequency components in these sequences which appear in the respective power spectra.

To frame the discussion in the later sections, we outline the design strategy of the various decoupling sequences. The new RF modulated decoupling schemes are built with TPPM as the building block. TPPM consists of two pulses of length τ with phases ϕ and $-\phi$. It is notated as $[\tau_\phi \tau_{-\phi}]$. Both τ and ϕ need to be experimentally optimised for maximum decoupling efficiency.

Taking $[\tau_\phi \tau_{-\phi}]$ as the building block, Fung and coworkers formulated a recipe which combines phase variations of the TPPM blocks and supercycling to obtain sequences of the SPINAL family [12]. The basic SPINAL scheme (SPINAL-8) has the form $[\tau_\phi \tau_{-\phi}][\tau_{\phi+\delta} \tau_{-(\phi+\delta)}][\tau_{\phi+2\delta} \tau_{-(\phi+2\delta)}][\tau_{\phi+\delta} \tau_{-(\phi+\delta)}]$, where ϕ and δ are respectively the starting value and the increment of the phase. Generally ϕ and δ are taken to be 10° and 5°, respectively, in which case SPINAL-8 reads as $[\tau_{10}\tau_{-10}][\tau_{15}\tau_{-15}][\tau_{20}\tau_{-20}][\tau_{15}\tau_{-15}]$. Notating the SPINAL-8 block as Q and defining $\overline{Q}$ as $[\tau_{-10}\tau_{10}][\tau_{-15}\tau_{15}]\ [\tau_{-20}\tau_{20}][\tau_{-15}\tau_{15}]$, SPINAL-16, SPINAL-32, and SPINAL-64 are obtained as $Q\overline{Q}$, $Q\overline{Q}\overline{Q}Q$, and $Q\overline{Q}\overline{Q}Q\overline{Q}Q\overline{Q}\overline{Q}$, respectively and which was called supercycling in the original report [12]. A reported advantage of SPINAL over TPPM is the need to experimentally optimise only the pulse length and not the phase. Here, with a goal to enhance the performance of SPINAL, we have relaxed this requirement and attempted to find the optimum value of both the initial phase (ϕ) and increment (δ) at various MAS rates. Earlier we had investigated the effect of the initial phase keeping the increment steps fixed at $\delta = 5^\circ$ and notated such sequences as SPINAL-64_x where x was the initial phase [21].

SW_f-TPPM is obtained by modulating the pulse length of TPPM blocks, i.e. by varying the values of τ. It can be represented by specifying the pulse width (τ) of each TPPM pair with the phase ϕ a constant and may be notated as $\{[0.78\tau_\phi 0.78\tau_{-\phi}][0.86\tau_\phi 0.86\tau_{-\phi}]$ $[0.94\tau_\phi 0.94\tau_{-\phi}][0.96\tau_\phi 0.96\tau_{-\phi}][0.98\tau_\phi 0.98\tau_{-\phi}][\tau_\phi \tau_{-\phi}][1.02\tau_\phi 1.02\tau_{-\phi}]$ $[1.04\tau_\phi 1.04\tau_{-\phi}]\ [1.06\tau_\phi 1.06\tau_{-\phi}][1.14\tau_\phi 1.14\tau_{-\phi}][1.22\tau_\phi 1.22\tau_{-\phi}]\}$. In other words, 11 TPPM blocks make up this sequence with the pulse lengths varying from 0.78τ to 1.22τ in the manner given above. Although the central pulse pair duration τ may have to be optimised for an enhanced performance, a value corresponding to flip angle of 180° suffices in most cases of practical interest. The numbers multiplying τ provide control over the profile of the sweep and a recipe to generate new sequences. In this fashion many profiles were designed by us, called SW_f-TPPM sequences in general, with qualitative differences in their power spectra.

The profiles of the new SW_f-TPPM analogues and their power spectra are given in Fig. 1 in the left and right columns, respectively. The numbers plotted on the ordinate in the left column of Fig. 1 are the multiplicative factors (denoted by f_i) that determine the profile. The numerical values are given in Table 1. We now summarise how the f_i's of the SW_f-TPPM family were obtained. All of them are composed of TPPM-like blocks with the central pulse pair having a pulse length close to that corresponding to a flip angle of 180°. The duration of the pulses in this block is denoted as 1.

- In $SW_f(\tau)$-TPPM the pulse widths were swept linearly from 0.75 to 1.25 times τ with an increment of 0.05. In equation form the f_i are given by $f_i = 0.75 + 0.05 \times (i-1)$ where i is the number of the TPPM block.
- The numerical factors of SW_f^{inv}-TPPM are given as $f_i = 1/x_i$ where x_i is given by $1.5 - 0.1 \times (i-1)$ and i in turn is the number of the TPPM block. In other words, x_i decreases linearly from 1.5 to 0.5.
- The two sequences $SW_f^{\tan_1}$-TPPM and $SW_f^{\tan_2}$-TPPM were generated by evaluating the function $1 + \tan\theta$ at 15 equidistant points as θ varied between $\approx -20^\circ$ and $\approx 20^\circ$ in the case of the former and between $\approx -14^\circ$ and $\approx 14^\circ$ in the latter. The case of

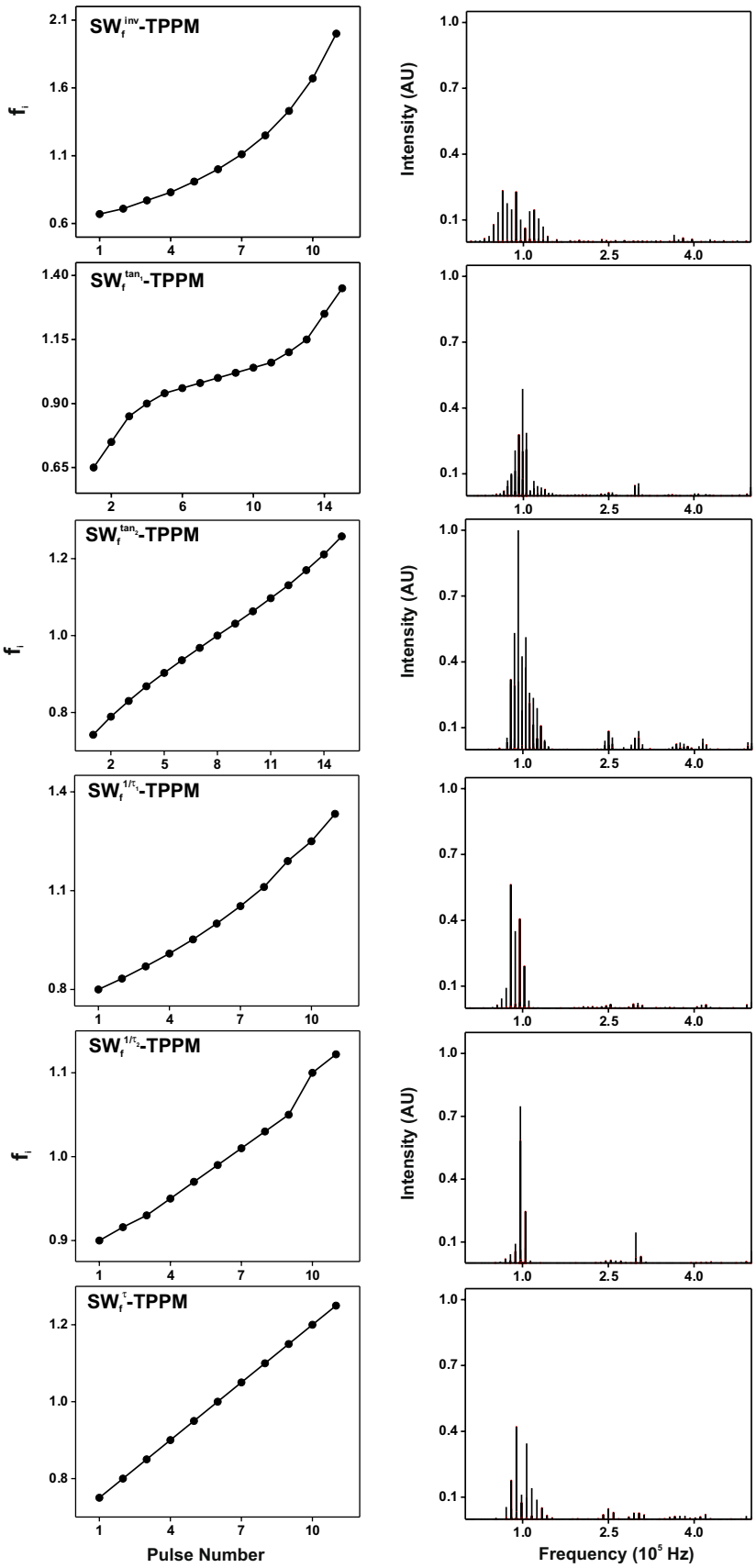

Fig. 1. The time and frequency profiles in the left and right columns, respectively of the various SW_f-TPPM analogues each of which was designed by repeating TPPM blocks with varying pulse lengths. The pulse length (normalised with respect to the central pulse pair) is plotted against the number of the TPPM block in the sequence.

Table 1
Pulse durations for various SW_f-TPPM (phase-modulated pulse length incremented) schemes

No.	SW_f-TPPM	SW_f^{inv}-TPPM	$SW_f^{tan_1}$-TPPM	$SW_f^{tan_2}$-TPPM	SW_f^{1/τ_1}-TPPM	SW_f^{1/τ_2}-TPPM	SW_f^{τ}-TPPM	$SW_f - TPPM_6$
1	0.78	0.67	0.65	0.742	0.900	0.800	0.75	0.85333
2	0.86	0.71	0.75	0.789	0.916	0.833	0.80	0.96
3	0.94	0.77	0.85	0.830	0.930	0.870	0.85	0.98667
4	0.96	0.83	0.90	0.868	0.950	0.909	0.90	1.01333
5	0.98	0.91	0.94	0.903	0.970	0.952	0.95	1.04
6	1.00	1.00	0.96	0.936	0.990	1.000	1.00	1.14667
7	1.02	1.11	0.98	0.968	1.010	1.053	1.05	
8	1.04	1.25	1.00	1.000	1.030	1.111	1.10	
9	1.06	1.43	1.02	1.031	1.050	1.190	1.15	
10	1.14	1.67	1.04	1.063	1.100	1.250	1.20	
11	1.22	2.00	1.06	1.097	1.122	1.333	1.25	
12			1.10	1.131				
13			1.15	1.170				
14			1.25	1.211				
15			1.35	1.258				

$SW_f - TPPM_6$ was similar with six equidistant points sampling the range $\approx -8^\circ$ to $\approx 8^\circ$. We note that $SW_f^{tan_1}$-TPPM is the same as the SW_f^{tan}-TPPM in our earlier study on a liquid-crystal [21].

- SW_f^{1/τ_1}-TPPM and SW_f^{1/τ_2}-TPPM are based on the $SW(1/\tau)$-FAM scheme used for the enhancement of the central-transition signal of half-integer spin quadrupolar nuclei [23]. Increasing the frequency components in a decoupling sequence with a fixed number of pulse pairs and hence a fixed cycle time requires the sweep width to be increased. A useful set of equations for this purpose, although originally introduced in the context of FAM, may be found in the work of Bräuniger et al. [23] which was adapted in the design of SW_f^{1/τ_1}-TPPM and SW_f^{1/τ_2}-TPPM with sweep widths of 22 and 50 kHz around the central RF field of 100 kHz.

3. Experimental

All experiments were performed on a Bruker AV500 MHz spectrometer equipped with a 2.5 mm double-resonance and a 4 mm triple-resonance CPMAS probes. The 2.5 mm probe was used for the study of the SPINAL decoupling sequence and the 4 mm probe was used for all the other studies. 5-CB was used for liquid-crystal studies with an RF field of 30 kHz applied for heteronuclear dipolar decoupling. For all the other studies natural abundance glycine was used. Spinning as well as static spectra were obtained by the ramped cross-polarisation technique [24].

4. Performance evaluation of SW_f-TPPM and its analogues

We now investigate the decoupling efficiency of SW_f-TPPM and its analogues and compare their performance with TPPM and SPINAL.

4.1. SW_f-TPPM

Fig. 2 shows an efficiency comparison of TPPM, SPINAL-64, and SW_f-TPPM on natural abundance glycine. The intensity of the C_α peak of glycine is plotted as a function of the MAS rate at RF power levels of 100, 90, and 70 kHz in the top row and as a function of pulse length, ^{1}H off-resonance, and phase respectively in the bot-

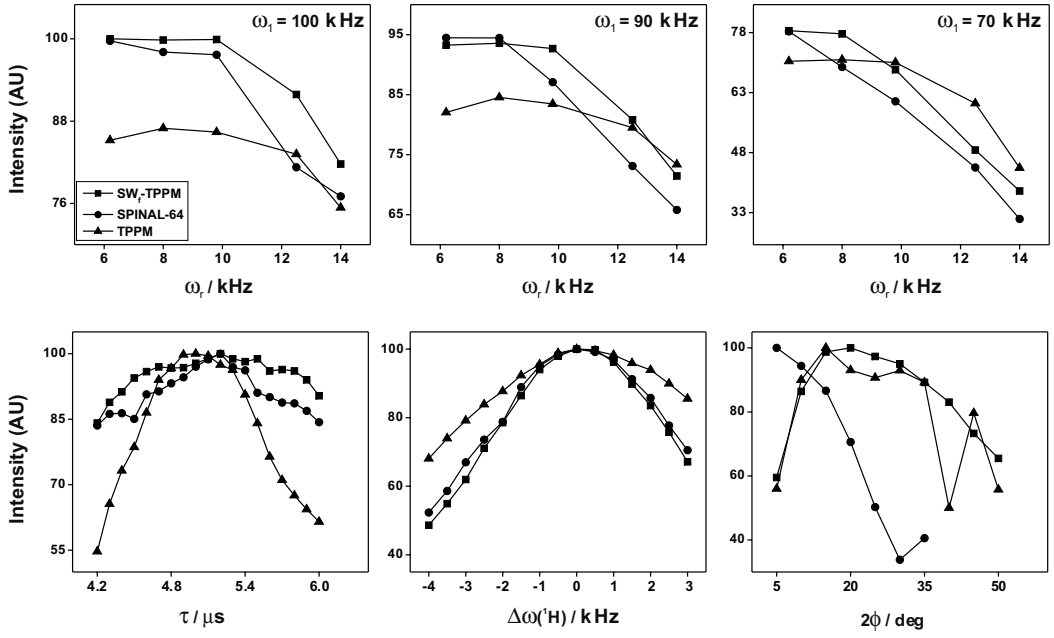

Fig. 2. Comparison of the decoupling efficiencies of TPPM, SPINAL-64, and SW_f-TPPM on natural abundance glycine. The top row shows the peak intensity of the CH_2 resonance of glycine at various MAS rates and RF fields of 100 kHz (left), 90 kHz (middle), and 70 kHz (right). The bottom row shows the intensity comparison as a function of the pulse length (τ), ^{1}H off-resonance ($\Delta\omega(^1H)$), and phase difference (2ϕ) from left to right at an RF field of 100 kHz and a MAS rate of 14 kHz. Data points for TPPM, SPINAL, and SW_f-TPPM are indicated by triangles (▲), circles (●), and squares (■), respectively.

tom row. Our earlier conclusions, based on a study of tyrosine [9], are borne out in that from a sensitivity standpoint SW_f-TPPM matches up favourably to TPPM and SPINAL-64 but shows improved robust performance with respect to τ and ϕ. The noticeable difference with the earlier study is the higher sensitivity of SW_f-TPPM to the ^{1}H off-resonance over TPPM and SPINAL-64. This sample-dependent phenomenon may arise from the reduced proton bath present in the sample under study compared to the earlier case of tyrosine [9].

For SW_f-TPPM the best performance was obtained when the cycle time τ_c was less than the rotor period τ_r. Fig. 3 shows the performance of TPPM, SPINAL-64, SW_f-TPPM, and $SW_f - TPPM_6$ as a function of ^{1}H off-resonance at a MAS rate of 14 kHz for RF fields of 100 and 80 kHz in the left and middle trace, respectively. The right trace shows the plot at a MAS rate of 8.8 kHz and RF field of 100 kHz. The cycle times of TPPM, SPINAL-64, SW_f-TPPM, and $SW_f - TPPM_6$ for 100 kHz of RF are 10, 80, 110, and 60 μs, respectively. A MAS rate of 14 kHz corresponds to a rotor period of 71.4 μs, thus, for this MAS rate with an RF of 100 kHz only TPPM and $SW_f - TPPM_6$ have $\tau_c < \tau_r$ and these two modulation schemes are found to be the least sensitive to ^{1}H off-resonance as seen in the left trace. For an RF field of 80 kHz, the cycle time of TPPM and $SW_f - TPPM_6$ becomes 12.5 and 75 μs, respectively and subsequently $SW_f - TPPM_6$ becomes very sensitive to ^{1}H off-resonance, as shown in the middle trace. When the MAS rate is lowered to 8.8 kHz with a rotor period of 113.6 μs and an RF Field of 100 kHz, τ_c for all the modulation schemes becomes smaller than τ_r and all the frequency-swept schemes become less sensitive to ^{1}H off-resonance than TPPM.

Experiments were done to check the efficiency of decoupling away from the *ideal* values of ϕ and τ for TPPM, SPINAL, and SW_f-TPPM. Fig. 4 shows the intensity of the C_α peak of glycine as

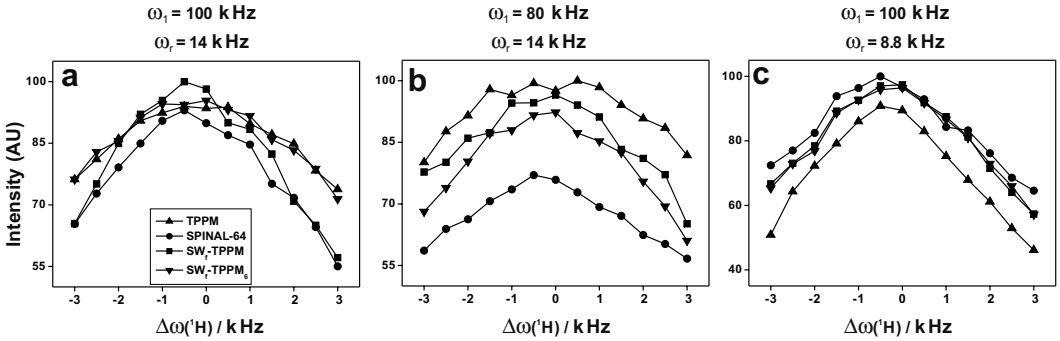

Fig. 3. Comparison of the decoupling efficiencies of TPPM, SPINAL-64, SW_f-TPPM, and $SW_f - TPPM_6$ on natural abundance glycine. The left and middle traces show the peak intensity of the CH_2 resonance of glycine at 14 kHz of MAS rate at RF fields of 100 and 70 kHz. The right trace corresponds to a MAS rate of 8.8 and 100 kHz of RF field. Data points for TPPM, SPINAL, SW_f-TPPM, and $SW_f - TPPM_6$ are indicated by triangles (▲), circles (●), squares (■), and inverted triangles (▼), respectively.

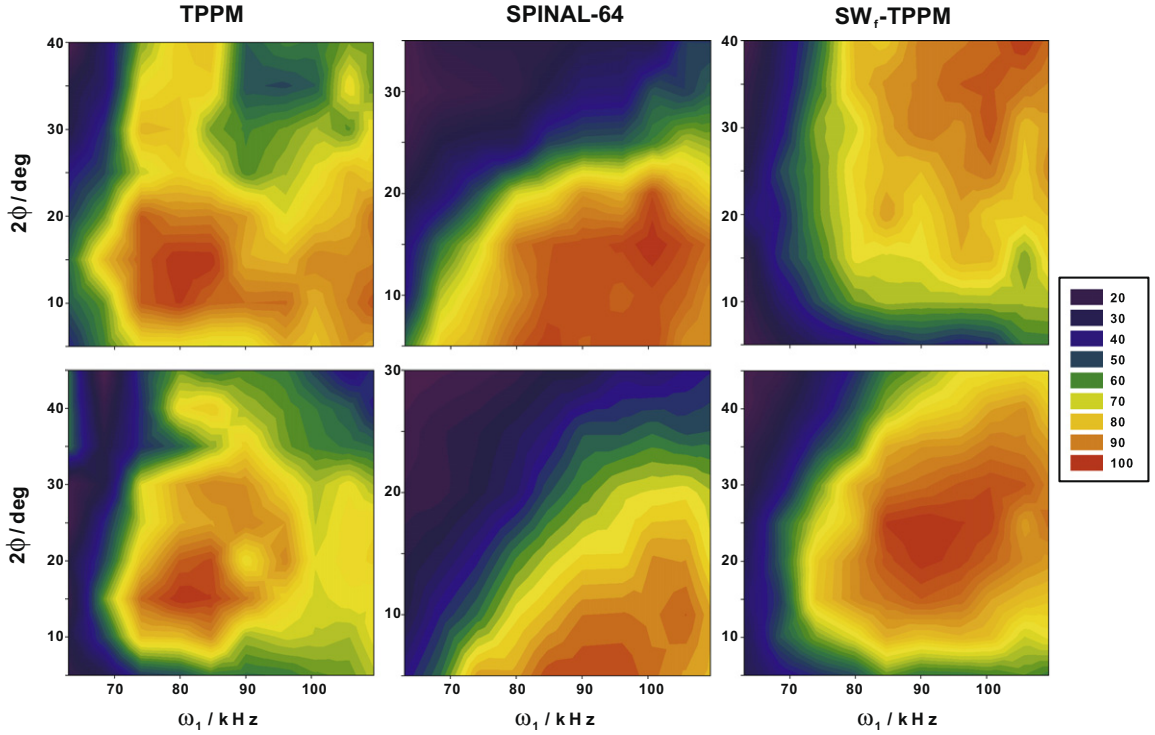

Fig. 4. The variation in the peak height of the CH_2 resonance of glycine during TPPM, SPINAL-64, and SW_f-TPPM decoupling measured as a function of the RF field ω_1 and phase difference 2ϕ (phase ϕ for SPINAL). The top row is for a MAS rate of 5.7 kHz and the bottom row is for 11.0 kHz. The phase-difference (2ϕ) values vary in 5° increments from 5°. The maximum values are 40° and 45° for SW_f-TPPM and TPPM at MAS frequencies of 5.7 and 11.0 kHz, respectively whilst for SPINAL-64 these are 35° and 30°, respectively. The RF fields taken are 63.0, 68.4, 74.0, 79.9, 84.7, 90.0, 96.1, 100.6, 105.8, and 109.5 kHz. The RF field strengths were measured with a nutation experiment on the ^{1}H resonance of adamantane.

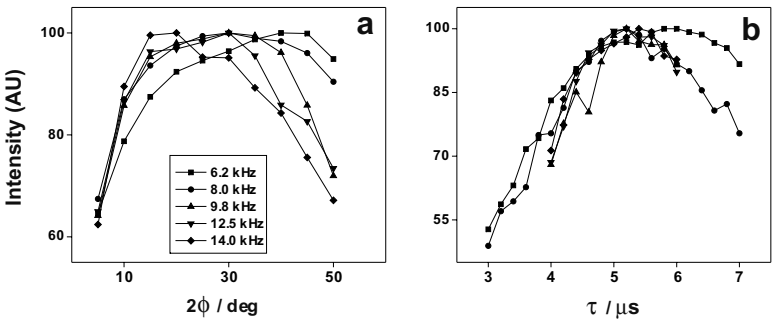

Fig. 5. SW_f-TPPM used for determining (a) the optimum phase and (b) the optimum pulse length for each rotor speed indicated in the plots for an RF field of 100 kHz. Peak height of CH_2 resonance of natural abundance glycine was measured in both the plots.

a function of the phase difference (2ϕ) and ^{1}H RF nutation frequency ω_1 (that in turn corresponds to the pulse length τ) for TPPM, SPINAL-64, and SW_f-TPPM for MAS rates of 5.7 kHz (top trace) and 11.0 kHz (bottom trace). The phase shown for SPINAL-64 here are the initial values keeping the increment same. The comparison shows that SPINAL-64 is more robust than TPPM which is clear for the lower MAS rate of 5.7 kHz where a broader area of efficiency is seen. The SPINAL performance becomes comparable to TPPM as the MAS rate increases. At the lower MAS rate of 5.7 kHz SW_f-TPPM is efficient at higher values of phase difference (2ϕ) not shown in the range depicted in Fig. 4 which is however evident in Fig. 5. At a MAS rate of 11.0 kHz the area of efficiency of decoupling has got quenched for all the methods with optimum ϕ for SPINAL-64 and SW_f-TPPM reduced significantly. This phenomenon can be attributed to the scaling of homonuclear ^{1}H–^{1}H couplings with increasing MAS rates, however, even at this MAS rate SW_f-TPPM is a much better method as it has a broader and homogeneous area of efficiency of decoupling. The influence of *II* couplings on *IS* decoupling will be dealt with in Section 4.3.

The robustness of SW_f-TPPM was studied at various MAS rates and the results are shown in Fig. 5. The aim was two fold: to find the optimum phase and pulse length values at various MAS rates and determine its effect on the decoupling efficiency. Fig. 5a and 5b compare the efficiency of SW_f-TPPM as a function of ϕ and τ, respectively at various spinning frequencies. The comparison clearly shows that the robustness of the method decreases with spinning frequency.

4.2. SW_f-TPPM Analogues

A comparison of the sequences in the SW_f-TPPM family will now be presented. It relies extensively on the results of Leskes et al. [11] the bare essentials of which are sketched below. The eigenvalues of the system Hamiltonian consisting of the chemical shift and heteronuclear dipolar coupling in the presence of a phase-modulated RF field is, according to the bimodal Floquet theory, given by

$$H_{00}^{\mp} = \frac{\Delta\omega^2}{k\omega_c} I_y \mp \frac{H_{CSA} \times H_{IS}}{n\omega_r + k\omega_c} I_y + \omega_1(\epsilon_x + \epsilon_y + \epsilon_z) I_p \qquad (1)$$

The difference in the eigenvalues of the H^+ and H^- Hamiltonians, corresponding to the ^{1}H spin being in the + or − states, is a measure of the efficiency of the decoupling. This was calculated for TPPM, SW_fTPPM,SW_f^{inv}TPPM,$SW_f^{1/\tau}$TPPM,SW_f^{1/τ_1}TPPM, and SW_f^{τ}-TPPM. The eigenvalues are measured as a function of the strength of the heteronuclear dipolar couplings $(\mathscr{H}_{DD}^{het})$ to mimic the effect of random orientation of crystallites. The result is plotted in Fig. 6. The difference for SW_f-TPPM and its analogues (except SW_f^{inv}-TPPM) is noticeably smaller than for TPPM. As this difference in eigenvalues manifests directly in line width, the large eigenvalue difference makes

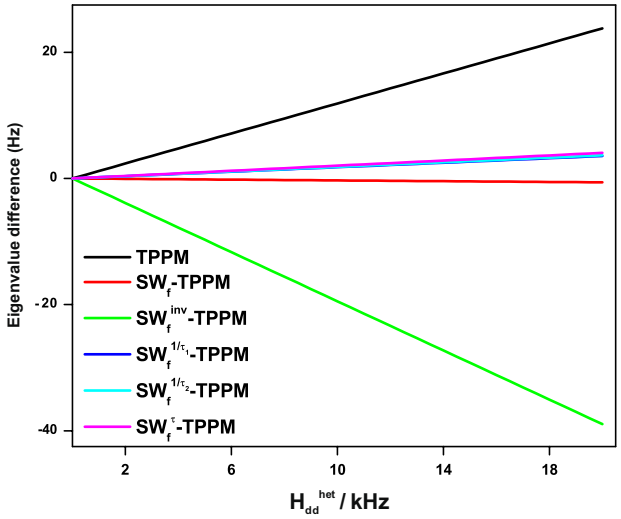

Fig. 6. The difference in the eigenvalues of H^+ and H^- Hamiltonian of Eq. 1 plotted for TPPM, SW_f-TPPM, SW_f^{inv}-TPPM, $SW_f(1/\tau)$-TPPM, SW_f^{1/τ_1}-TPPM, and $SW_f^{\tau_2}$-TPPM as a function of strength of the heteronuclear dipolar coupling $(\mathscr{H}_{DD}^{het})$ to mimic the effect of random orientation of crystallites. Homonuclear dipolar coupling among the ^{1}H spins was not considered here.

SW_f^{inv}-TPPM less efficient at higher spinning speed (see Fig. 7). Profiles where the pulse-width modulation are symmetric (SW_f-TPPM, SW_f^{1/τ_1}-TPPM, SW_f^{1/τ_2}-TPPM, and SW_f^{τ}-TPPM) are better behaved with SW_f-TPPM outperforming the others, presumably due to its adiabatic character.

Extensive comparison of the sequences in the group were also carried out. In Fig. 7, the efficiency of the SW_f-TPPM family is compared as a function of the pulse length and phase. One can notice in this figure that all the sequences work over a range of pulse lengths and phase, in other words they are robust, and their robustness scales with the sweep width. The most robust amongst these is SW_f^{inv}-TPPM which has the largest sweep width in the power spectrum. Its robust performance is most likely a result of the decoupling resonance conditions, alluded to earlier, being satisfied over the course of the sweep. Such resonance conditions have been invoked earlier to explain the efficiency of SPINAL [11]. The efficiency of SW_f^{inv}-TPPM, however, deteriorates with spinning speed.

4.3. Influence of ^{1}H–^{1}H couplings on ^{13}C–^{1}H decoupling

One of the main drawbacks of CW decoupling is the deterioration of its efficiency with increasing spinning speed. This was one of the aspects considered whilst sophisticated sequences were designed. An understanding of the interference of ^{1}H–^{1}H dipolar

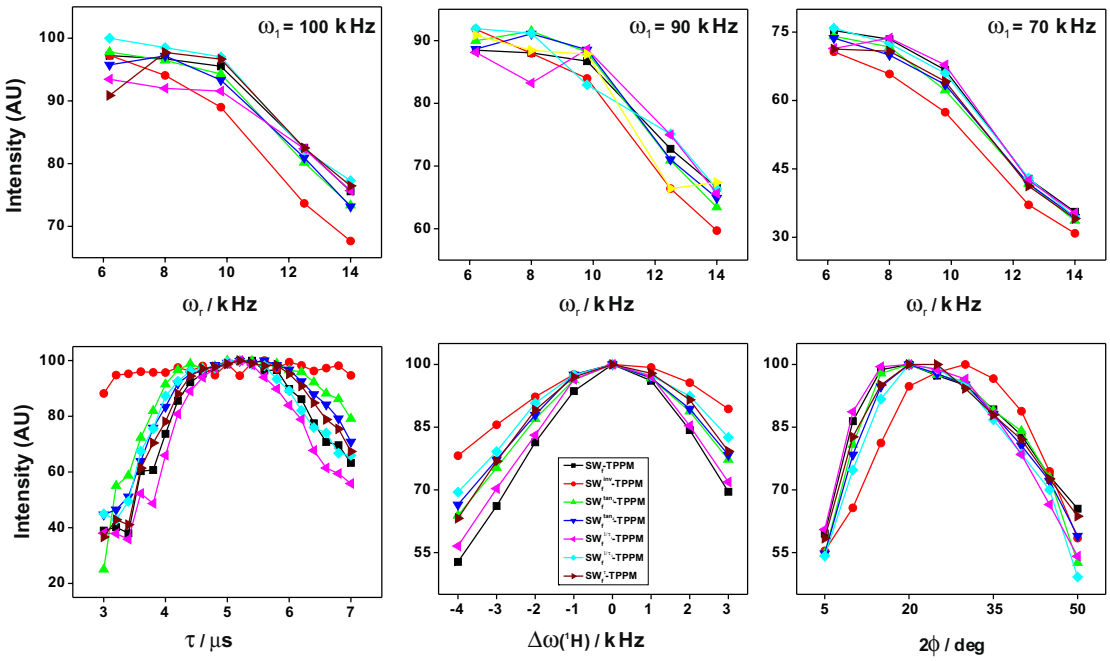

Fig. 7. Efficiency and robustness of various SW_f-TPPM analogues. The top row shows peak intensity of CH_2 resonance of glycine plotted at various MAS rates at RF fields of 100 kHz (left), 90 kHz (middle), and 70 kHz (right). The bottom row shows a similar comparison as a function of pulse length (τ), ^{1}H off-resonance ($\Delta\omega(^1H)$), and phase difference (2ϕ) and from left to right. The robustness comparison was done at an RF field of 100 kHz and MAS rate of 14 kHz.

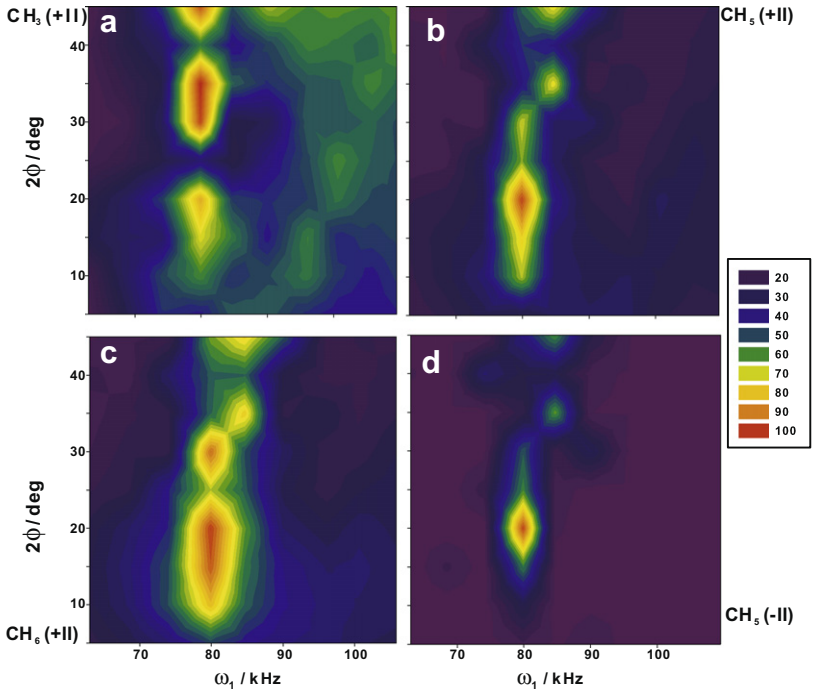

Fig. 8. The peak intensity of ^{13}C of isobutyl skeleton simulated with various spin systems, namely, CH_3, CH_5, CH_6 (with II couplings), and CH_5 (without II couplings) with TPPM decoupling. The simulations were done at a MAS rate of 5.818 kHz and pulse length of $\tau = 6.25$ μs by varying phase difference (2ϕ, along *Y*-axis) and RF field (ω_1, along *X*-axis). Phase difference (2ϕ) was varied from 5° to 45° in steps of 5°. The RF field strengths taken are those implemented in experiments (shown in Fig. 2) i.e. 63.0, 68.4, 74.0, 79.9, 84.7, 90.0, 96.1, 100.6, 105.8, and 109.5 kHz.

coupling with heteronuclear dipolar decoupling was recently obtained with bimodal Floquet theory [11]. Simulations are performed here to further probe the role of a dipolar bath made up of ^{1}H–^{1}H couplings by measuring the intensity of a ^{13}C bonded to n ^{1}H nuclei. The simulations were performed with SPINEVOLUTION [25] owing to its ability to handle large spin systems. Co-ordinates and NMR parameters of spin systems CH_1 to CH_9 provided in the package were used in these simulations. The simulations shown in Figs. 8 and 9 (considering TPPM and SW_f-TPPM, respectively at a MAS rate of 5.8 kHz) were done to verify the experimental

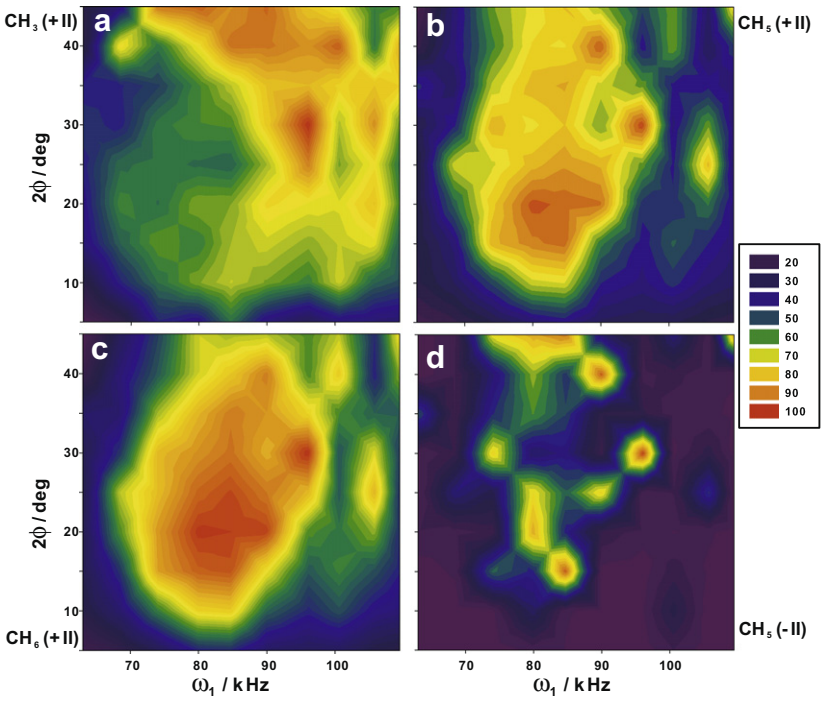

Fig. 9. The peak intensity of ^{13}C resonance of isobutyl skeleton simulated with various spin systems, namely, CH_3, CH_5, CH_6 (with II couplings), and CH_5 (without II couplings) with SW_f-TPPM decoupling. The rest of the parameters are as in Fig. 8.

observation in Fig. 3 with various spin systems, namely, CH_3, CH_5, and CH_6 with *II* couplings and CH_5 without *II* couplings. The area of efficient decoupling increases with the size of the spin system (CH_3, CH_5, and CH_6 with *II* couplings) and the effect is more pro-

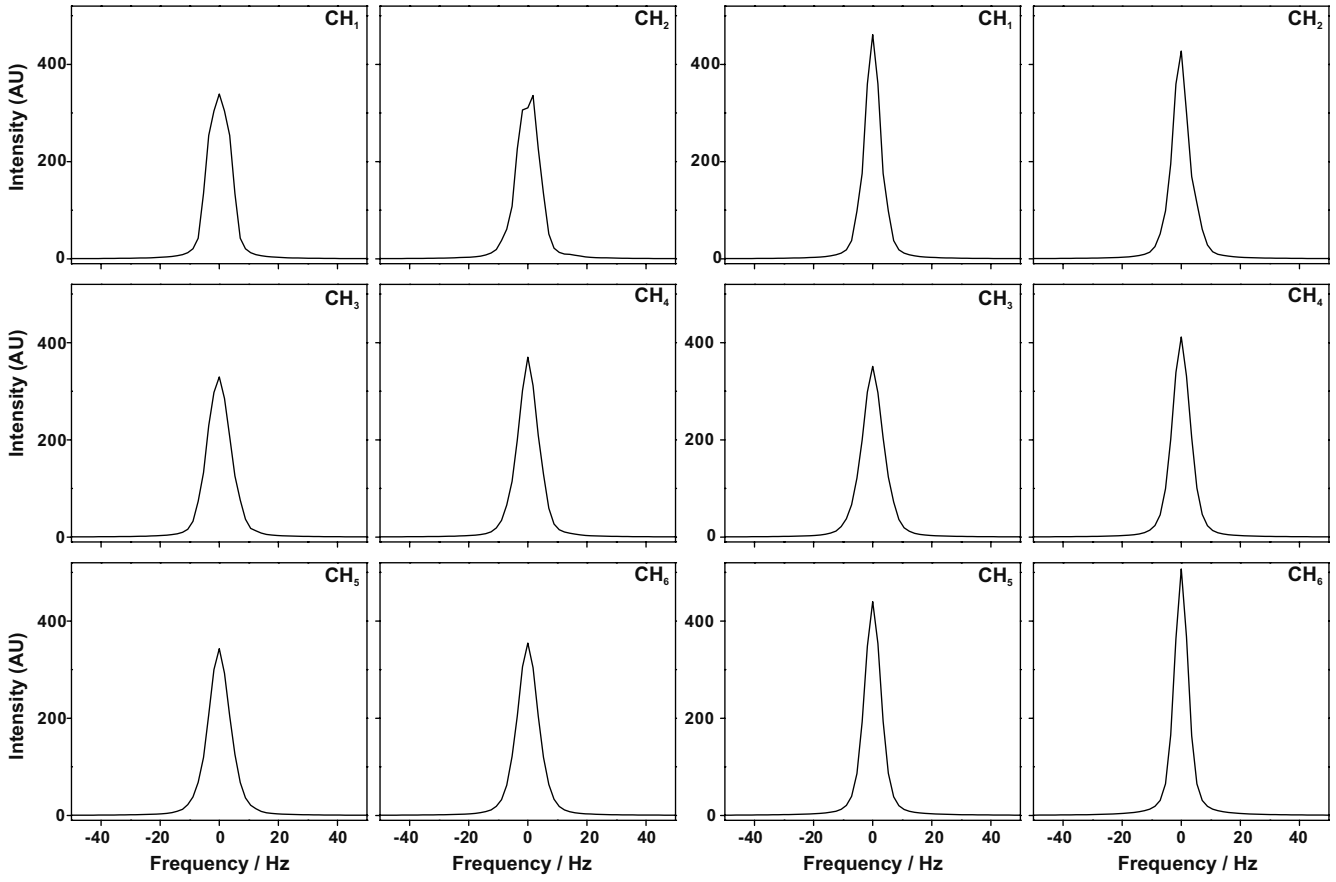

Fig. 10. The spectra of isobutyl skeleton simulated with various spin systems at a MAS rate of 5.8 kHz taking a pulse length of 6.25 μs. The spectra of CH_1 to CH_6 are simulated with TPPM (first and second columns at optimum RF field of 79 kHz and phase difference of 20°) and SW_f-TPPM (third and fourth columns at optimum RF field of 81 kHz and phase difference of 20°).

nounced for SW_f-TPPM than for TPPM. One can also observe that the same area shrinks severely if *II* couplings are removed in the simulation, as shown for CH_5, indicating that the robustness is affected heavily by *II* couplings. Its effect on SW_f-TPPM is more as the sequence itself relies on adiabaticity for robust performance and any additional mechanism, like ^1H–^1H couplings, can aid it favourably. At moderate MAS rates in real-life spin systems the strongly coupled *II* bath can aid both TPPM and SW_f-TPPM with the latter expected to gain more due to additional resonance condition matchings. This intuition is evident in Fig. 10 where the spectrum at MAS of 5.7 kHz with both TPPM (left column) and SW_f-TPPM (right column) improves with larger spin systems with SW_f-TPPM outperforming TPPM. The simulations are performed for optimum values of RF field and phase difference (2ϕ), mentioned in the figure caption. Simulations were performed for nominal RF field of 80 kHz (corresponding to 180° for the pulse flip angle) and phase difference of 20° (data not shown) which lead to line shapes without splitting for larger spin systems whilst smaller spin systems showed line shapes with splittings. These splittings are due to inefficient heteronuclear dipolar decoupling whilst in the case of larger spin systems the homonuclear dipolar couplings mitigate this effect. Good line shapes for small spin systems are obtained only at optimum flip angle and phase, whereas the lineshape and intensity remain unaffected for larger spin systems for nominal values. Numerical description of smaller spin systems needs precise setting of flip angle and phase. The numerical optimum value of the flip angle and the phase for spin systems were found to be different at different MAS rates.

As the MAS rate increases, the strength of the *II* couplings is reduced due to the averaging and the beneficial effects it has on decoupling disappear. This phenomenon was noted and investigated in some detail by Ernst et al. [10]. We find that at a MAS rate of 11.6 kHz, Fig. 11, the peak height increases with the size of the spin system till CH_4. Any further increase in the spin system leads to a slow decrease in the peak intensity. Interestingly enough, the baseline of the spectra broadens at higher MAS rates for higher spin systems (for larger values of n in SI_n), which is the realistic situation. Such an observation was reported for TPPM by Ernst et al. who also reported that the XiX decoupling scheme improved this aspect resulting in significant intensity enhancement [19]. A further increase in the broad baseline is observed for simulations done at 17.4 kHz, Fig. 12, where the broad baseline appears at even smaller size of the spin systems and peak height obtained with SW_f-TPPM is discouraging. This shows that the SW_f-TPPM will deteriorate around this MAS rate and the trend will continue for higher MAS rates. However, we believe that it can be overcome by a suitable design of the sweep profile and work is being done along this direction.

5. Significance of phase in SPINAL performance

As already mentioned SPINAL was designed as TPPM blocks repeated with variations in the phase. In SPINAL-8 the four TPPM blocks normally have phases (10, −10), (15, −15), (20, −20), and (15, −15). The higher analogues were designed by supercycling as outlined earlier. If the phases of the TPPM blocks are plotted

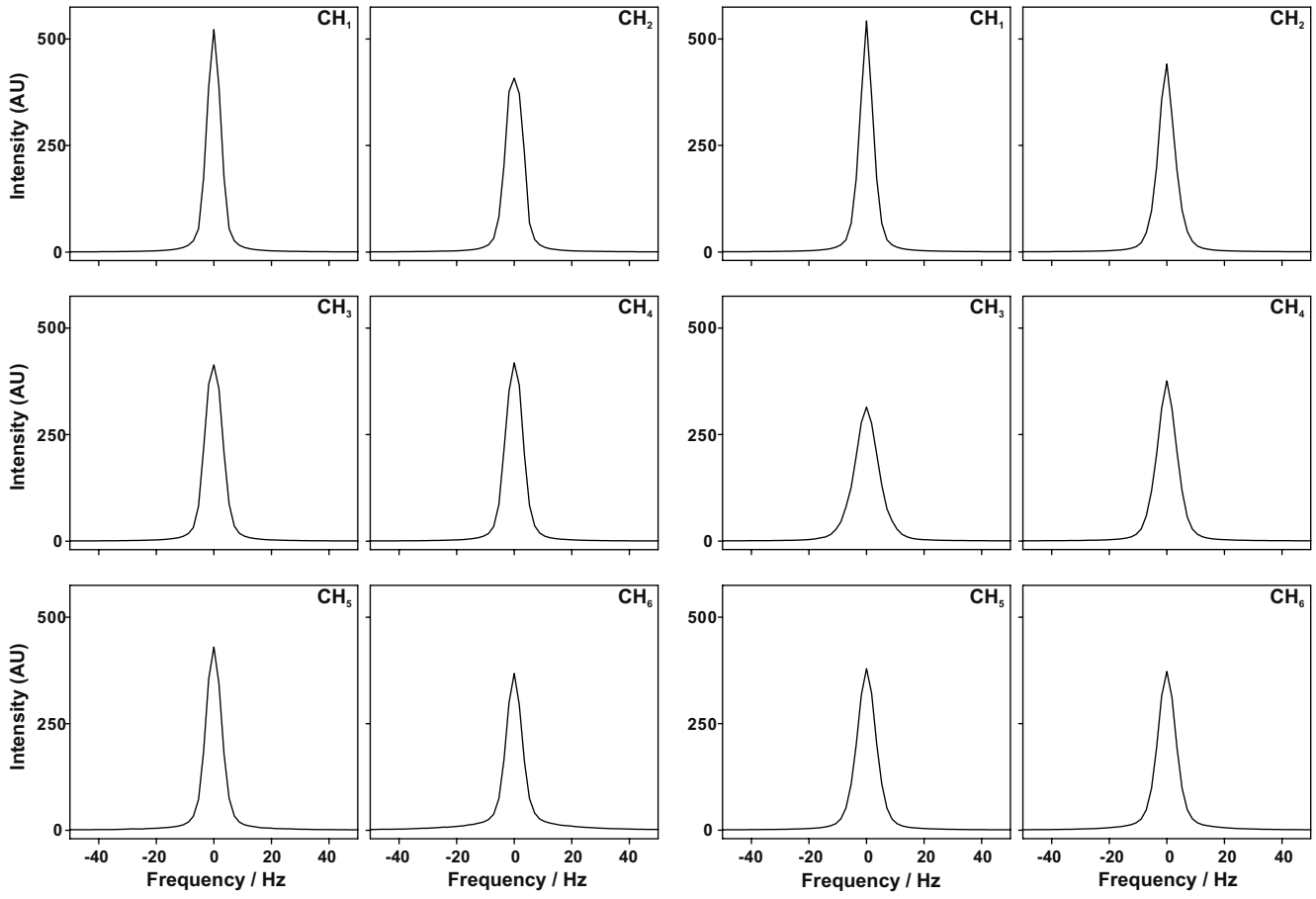

Fig. 11. The spectra of isobutyl skeleton simulated with various spin systems at a MAS rate of 11.6 kHz taking a pulse length of 6.25 μs. The spectra of CH_1 to CH_6 are simulated with TPPM (first and second columns at optimum RF field of 80 kHz and phase difference of 18°) and SW_f-TPPM (third and fourth columns at optimum RF field of 83 kHz and phase difference of 20°).

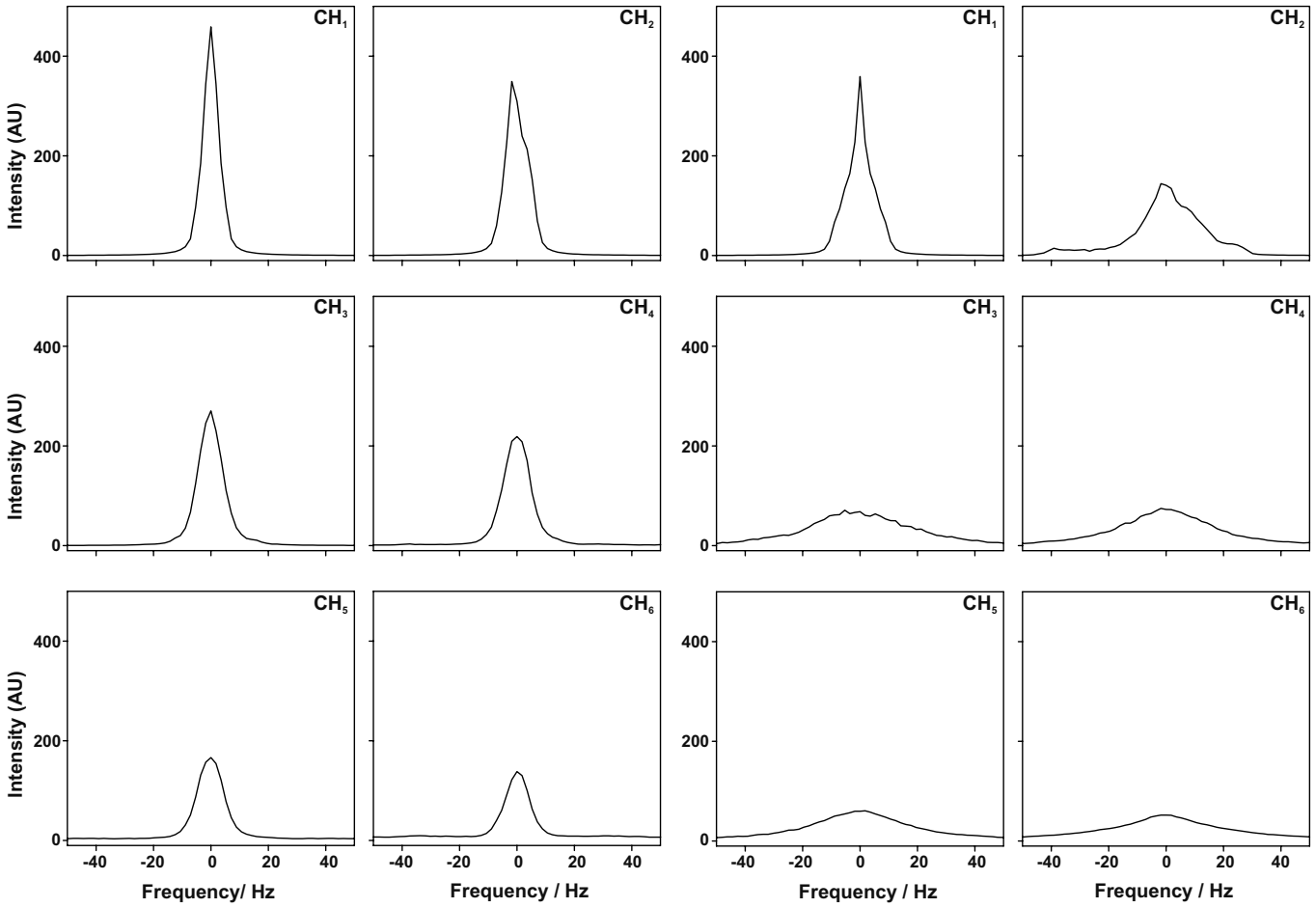

Fig. 12. The spectra of isobutyl skeleton simulated with various spin systems at a MAS rate of 17.4 kHz taking a pulse length of 6.25 μs. The spectra of CH_1 to CH_6 are simulated with TPPM (first and second columns at optimum RF field of 85 kHz and phase difference of 48°) and SW_f-TPPM (third and fourth columns at optimum RF field of 97 kHz and phase difference of 50°).

against their order of occurrence, the profile of SPINAL-8 resembles three-quarters of a Gaussian.

In addition to the pulse length which is the only parameter that is normally optimised in SPINAL, the initial phase ϕ and the phase increment step δ could also be allowed to vary. In the original report the initial phase ($\phi = 10^\circ$) and phase increment ($\delta = 5^\circ$) were defined and fixed but this combination was found to be sub-optimal in our earlier studies [9,21].

We now report results from our investigation on the performance of SPINAL-8 and SPINAL-64 with different ϕ and δ. The maximum value of the initial phase that we have studied is 5° which was found to be better than larger values. Fig. 13 shows the efficiency comparison of SPINAL-8 scheme as a function of δ for initial ϕ values of 1°, 3° and 5° at MAS rates of 5, 10, 15, and 20 kHz. The first striking observation is that the recommended step size of 5° is not the optimum for all cases and depends upon the initial phase as well as on the MAS rates. The optimum combination is not significant for the lower MAS rate of 5 kHz but becomes more important for higher MAS rates and is extremely critical for the high MAS rate of 20 kHz. This is understandable in the light of robustness created by strong ^1H–^1H couplings. The most efficient point in these curves are comparable to *regular* SPINAL-64 (data not shown) which suggest that *supercycling* is perhaps not very critical.

Our experimental investigations suggest that besides pulse length (τ), the initial phase (ϕ) and phase increment step (δ) need to be optimised for increasing the efficiency of SPINAL scheme. The optimum value of both these parameters depends on the spinning speed.

6. Decoupling in liquid crystal: role of phase

In an earlier study, TPPM based phase-modulated heteronuclear decoupling sequences were applied on a liquid-crystal and were shown to improve the spectra [21]. In particular, we found that SPINAL-64_{15} was more robust than SPINAL-64_{10}. Additionally, SW_f-TPPM sequences were found to perform better at higher phase ($2\phi = 40^\circ$) than the regular values of $2\phi = 25^\circ$. Moreover, the dependence of these sequences on the ^1H offset depended on the value of ϕ taken [21].

Results of a systematic study on the interplay of the phase and the proton offset on the decoupling efficiency monitoring the C_α peak of 5-CB are shown in Fig. 14. Fig. 14a shows the off-resonance behaviour of SPINAL-64_{10}, SPINAL-64_{15}, $SW_f - TPPM_{25}$, $SW_f^{inv} - TPPM_{25}$, $SW_f^{inv} - TPPM_{40}$, $SW_f^{tan_1} - TPPM_{25}$, and $SW_f^{tan_1} - TPPM_{40}$, the number on the subscript showing the phase (ϕ for SPINAL) and phase difference (2ϕ) for SW_f-TPPM schemes chosen for the modulation under the study. This comparison indicates that higher values of the phase have improved off-resonance behaviour whilst the lower values of phase are more efficient on resonance. We have also attempted the reverse, that is, determining the optimum value of the phase difference (2ϕ) for various off-resonance positions. Fig. 14b shows the comparison of decoupling efficiency of various sequences as a function of the phase

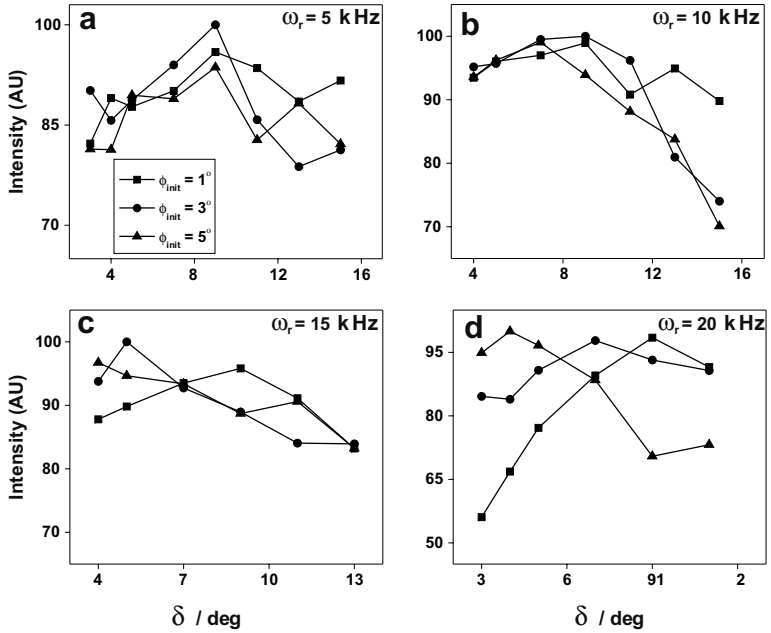

Fig. 13. The decoupling efficiency of SPINAL-8 block compared as a function of the step size (δ) at various MAS rates. The initial value of the phase (ϕ_{init}) was 1°, 3°, and 5° for square (■), circle (●), and triangle (▲) respectively. The RF field was 90 kHz.

difference for on-resonance decoupling. Smaller values of phase are more efficient in this situation. With the carrier offset by 400 and 800 Hz, the results, shown in Fig. 14c and 14d, respectively indicate that the optimum value of phase moves towards higher values gradually.

It can be seen that at on-resonance SPINAL-64_{10} performs better than SPINAL-64_{15} with the latter showing better ^{1}H off-resonance characteristics. The SW_f-TPPM sequences also showed similar behaviour with $SW_f - TPPM_{40}$ having much better ^{1}H off-resonance characteristics than $SW_f - TPPM_{25}$ although the intensity is slightly lower at the optimum ^{1}H offset. It should be noticed that SW_f-TPPM and its analogues are more immune to this trend. The tolerance to off-resonance is important as in any system there can be more than one ^{13}C resonance that are sensitive to decoupling of ^{1}H nuclei. Better off-resonance behaviour of decoupling sequence ensures an overall improvement in sensitivity and

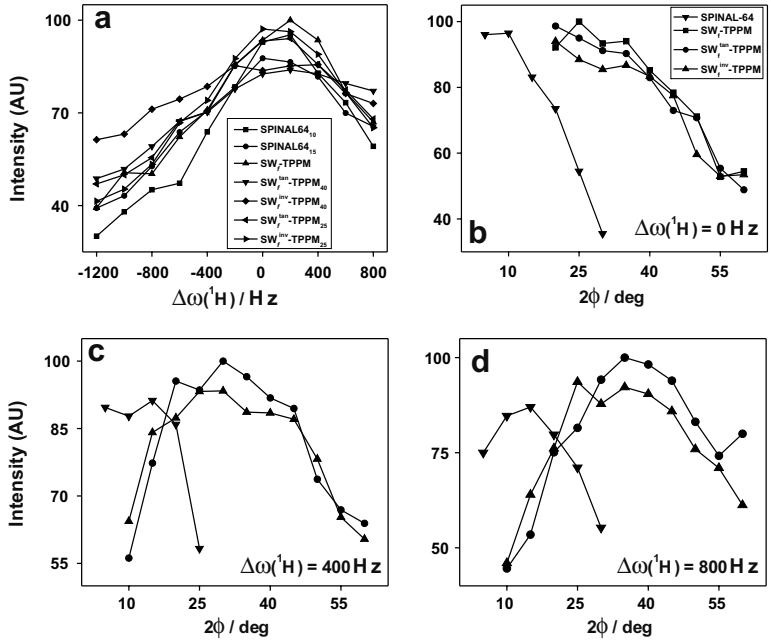

Fig. 14. Intensity of the C_α peak of 5-CB obtained with various decoupling sequences. (a) The off-resonance behaviour of SPINAL-64_{10}, SPINAL-64_{15}, SW_fTPPM$_{25}$, $SW_f^{inv} - TPPM_{25}$, $SW_f^{inv} - TPPM_{40}$, $SW_f^{tan_1} - TPPM_{25}$, and $SW_f^{tan_1} - TPPM_{40}$. The spectra were acquired with cross-polarisation under static condition and ω_1 of 30 kHz was used for decoupling. (b) The efficiency of decoupling as a function of phase for SPINAL-64, SW_f-TPPM, SW_f^{inv}-TPPM, and $SW_f^{tan_1}$-TPPM under on-resonance condition. (c and d) The comparison of efficiency of decoupling at off-resonance values of 400 and 800 Hz, respectively as a function of phase for SPINAL-64, SW_f^{inv}-TPPM, and SW_f^{tan}-TPPM. (b–d) Share the same set of legends for sequences where SPINAL-64, SW_f-TPPM, SW_f^{inv}-TPPM, and SW_f^{tan}-TPPM are denoted by inverted triangle (▼), square (■), triangle (▲), and circle (●), respectively.

resolution of the spectra which were realised with SW_f-TPPM sequences [21].

To summarise the results, it is advisable to use $SW_f - TPPM_\phi$, $SW_f^{inv} - TPPM_\phi$, and $SW_f^{tan} - TPPM_\phi$ with higher value of 2ϕ, (say 30–40°) or SPINAL-64_{15} which allows the carrier frequency to be kept slightly away (0.5–1.0 kHz) from C_α without much loss in the intensity in the case of samples under static conditions for heteronuclear dipolar decoupling.

7. Conclusions

We have designed decoupling sequences by modulating the pulse length of TPPM blocks. This simple approach has produced effective decoupling schemes that are easy to implement. It was found that robustness of decoupling depends upon the nature of the sample itself and degrades with the MAS rate. Both of these observations can be explained on the basis of II couplings. The simulations show that II couplings lead to a robust performance for these sequences and enhanced peak intensity for higher spin systems. The simulations also show a broadening of the baseline for higher spin systems.

Various SW_f-TPPM sequences based on different sweep profiles have been designed and tested and it was found that at lower MAS rates, the details of the profile are not critical. Robust performance can be realised by designing a SW_f-TPPM scheme with a large sweep width. A detailed investigation of frequency-modulated decoupling sequences was done. These sequences are robust with experimental parameters and robustness being tunable at lower MAS rates.

SPINAL enjoys widespread popularity because it is easy to use and optimise with improved efficiency to TPPM. We have investigated the effect of varying the initial phase and the phase increment on the decoupling efficiency of SPINAL. Our study shows that improved performance can be achieved by manipulating the initial phase and increment steps with SPINAL-8 optimised in this fashion having comparable performance to supercycled SPINAL-64.

The liquid-crystal study suggests that robustness towards off-resonance of the modulated TPPM sequences (SW_f-TPPM sequences and SPINAL-64) improves with increasing depth of the phase modulation with marginal loss of efficiency. For such systems, it is advisable to work with an optimum phase difference (2ϕ) of 30–40° for SW_f-TPPM sequences and phase of (ϕ) 15° for SPINAL-64.

Acknowledgments

PKM acknowledges assistance from Department of Science and Technology, India, under SERC FAST Track Scheme. NDK thanks TIFR for support during a sabbatical stay when a major part of the work was accomplished. We acknowledge Mr. Manoj Naik for technical assistance, and the use of the National Facility for High Field NMR, TIFR, Mumbai.

References

[1] U. Haeberlen, High Resolution NMR in Solids: Selective Averaging, Academic Press, New York, 1976.
[2] M. Mehring, High Resolution NMR in Solids, Springer, Berlin, 1976.
[3] M. Duer, Introduction to Solid-State NMR Spectroscopy: Principles and Applications, Blackwell Sciences, U.K, 2002.
[4] A.L. Bloom, J.N. Shoolery, Effects of perturbing radiofrequency fields on nuclear spin coupling, Phys. Rev. 97 (1955) 1261–1265.
[5] A.E. Bennett, C.M. Rienstra, M. Auger, K.V. Lakshmi, R.G. Griffin, Heteronuclear decoupling in rotating solids, J. Chem. Phys. 103 (1995) 6951–6958.
[6] M. Ernst, Heteronuclear spin decoupling in solid-state NMR under magic-angle sample spinning, J. Magn. Reson. 162 (2003) 1–34.
[7] P. Hodgkinson, Heteronuclear decoupling in the NMR of solids, Prog. NMR Spectr. 46 (2005) 159–184.
[8] K. Riedel, C. Herbst, J. Leppert, O. Ohlenschläger, M. Görlach, R. Ramachandran, Heteronuclear decoupling in rotating solids: Improving the efficacy of CN_m^n symmetry-based $\frac{\tanh}{\tan}$ adiabatic RF pulse schemes, Chem. Phys. Lett. 429 (2006) 590–594.
[9] R.S. Thakur, N.D. Kurur, P.K. Madhu, Swept-frequency two-pulse phase modulation for heteronuclear dipolar decoupling in solid-state NMR, Chem. Phys. Lett. 426 (2006) 459–463.
[10] M. Ernst, H. Zimmermann, B.H. Meier, A simple model for heteronuclear spin decoupling in solid-state NMR, Chem. Phys. Lett. 317 (2000) 581–588.
[11] M. Leskes, R.S. Thakur, P.K. Madhu, N.D. Kurur, S. Vega, A bimodal Floquet description of heteronuclear decoupling in solid-state nuclear magnetic resonance, J. Chem. Phys. 127 (2007) 0245601.
[12] B.M. Fung, A.K. Khitrin, K. Ermolaev, An improved broadband decoupling sequence for liquid crystals and solids, J. Magn. Reson. 142 (2000) 97–101.
[13] G.D. Paëpe, A. Lesage, L. Emsley, The performance of phase-modulated heteronuclear dipolar decoupling schemes in fast magic-angle-spinning nuclear magnetic resonance experiments, J. Chem. Phys. 119 (2003) 4833–4841.
[14] G.D. Paëpe, N. Giraud, A. Lesage, P. Hodgkinson, A. Böckmann, L. Emsley, Transverse dephasing optimized solid-state NMR spectroscopy, J. Am. Chem. Soc. 125 (2003) 13938–13939.
[15] G. Gerbaud, F. Ziarelli, S. Caldarelli, Increasing the robustness of heteronuclear decoupling in magic-angle sample spinning solid-state NMR, Chem. Phys. Lett. 377 (2000) 1–5.
[16] A. Khitrin, B.M. Fung, Design of heteronuclear decoupling sequences for solids, J. Chem. Phys. 112 (2000) 2392–2398.
[17] M. Eden, M. Levitt, Pulse sequence symmetries in the nuclear magnetic resonance of spinning solids: application to heteronuclear decoupling, J. Chem. Phys. 111 (1999) 1511–1519.
[18] M.H. Levitt, Encyclopedia of Nuclear Magnetic Resonance, vol. 9, Wiley, UK, 2002. pp. 165.
[19] A. Detken, E.H. Hardy, M. Ernst, B.H. Meier, Simple and efficient decoupling in magic-angle spinning solid-state NMR: the XiX scheme, Chem. Phys. Lett. 356 (2002) 298–304.
[20] P. Tekely, P. Palmas, D. Canet, Effect of proton spin exchange on the residual ^{13}C MAS NMR linewidths Phase-modulated irradiation for efficient heteronuclear decoupling in rapidly rotating solids, J. Magn. Reson. A 107 (1994) 129–133.
[21] R.S. Thakur, N.D. Kurur, P.K. Madhu, Improved heteronuclear dipolar decoupling sequences for liquid-crystal NMR, J. Magn. Reson. 185 (2007) 264–269.
[22] R.S. Thakur, N.D. Kurur, P.K. Madhu, Improved decoupling sequences for MQ-MAS and HR-MAS applications in solid-state NMR, Magn. Reson. Chem. 46 (2008) 166–169.
[23] T. Bräuniger, G. Hempel, P.K. Madhu, Fast amplitude-modulated pulse trains with frequency sweep (SW-FAM) in static NMR of half-integer spin quadrupolar nuclei, J. Magn. Reson. 181 (2006) 68–78.
[24] G. Metz, X. Wu, S.O. Smith, Ramped-amplitude cross polarization in magic-angle-spinning NMR, J. Magn. Reson. A 110 (1994) 219–227.
[25] M. Veshtort, R.G. Griffin, SPINEVOLUTION: a powerful tool for the simulation of solid and liquid state NMR experiments, J. Magn. Reson. 178 (2006) 248–282.